

Randomized resolvent analysis

Jean Hélder Marques Ribeiro¹†, Chi-An Yeh¹, and Kunihiko Taira¹

¹Department of Mechanical and Aerospace Engineering, University of California, Los Angeles, CA 90095, USA

(Received xx; revised xx; accepted xx)

Discretization of the Navier–Stokes equations to perform resolvent analysis of fluid flows requires us to handle a large operator, especially for high-Reynolds-number turbulent flows. Despite the need of only extracting a few dominant resolvent and forcing modes, the resolvent analysis necessitates the large resolvent operator to be analyzed. Here, we consider the use of randomized numerical linear algebra to reduce the dimension of the resolvent operator for achieving computational speed up and memory saving compared to the standard resolvent analysis. To accomplish this goal, we utilize sketching of the linear operator with a random Gaussian test matrix and perform singular value decomposition on a low-rank matrix holding dominant characteristics of the full resolvent operator. The strength of the randomized resolvent analysis is demonstrated on a turbulent separated flow over an airfoil. This randomized approach clears the path towards tackling resolvent analysis for higher-Reynolds number and tri-global base flows.

Key words: resolvent analysis, instabilities, randomized methods

1. Introduction

One of the central questions in turbulence and flow control is concerned with the evolution of perturbations. Gaining detailed understanding of the perturbation dynamics in turbulent flows is a daunting task, due to the complex nonlinear dynamics that takes place over a broad range of spatial and temporal scales. To modify the global flow characteristics with control, it is necessary that the nonlinear interactions involving the actuation input (perturbation) become appropriately large to alter the base flow. For flow control, we need not track all possible ways in which the actuation input can modify the flow, but instead we can focus on the dominant directions in which the perturbation can be amplified. This notion has led to the modal analysis based approaches (Holmes *et al.* 2012; Schmid & Henningson 2001; Taira *et al.* 2017), including the global stability analysis (Theofilis 2011) and the resolvent analysis (Trefethen *et al.* 1993).

In the presence of sustained perturbations or forcing inputs, the linear system response can be described by the transfer function from control theory. This linear analysis is greatly simplified when the input to the system is sinusoidal and leads to the well-known Bode plots that reveal the gain and phase response of the system over a range of forcing frequencies. The transfer function that relates the system input to the output is called the resolvent and its analysis has been extended to fluid flows by Trefethen *et al.* (1993). The resolvent analysis is based on the pseudospectral analysis and has been used to study the transient energy growth (Trefethen *et al.* 1993) as well as the harmonic response of the system (Jovanović & Bamieh 2005). These initial studies of resolvent analysis were performed about stable laminar flows.

A breakthrough in the approach to analyze turbulent flow was introduced by McKeon & Sharma (2010). They considered the nonlinear advection term to be the self-sustained

† Email address for correspondence: jeanmarques@ucla.edu

input within the natural feedback loop of the fluid flow. This viewpoint has enabled the use of time-averaged base flows to reveal the input-output dynamics of turbulent flows. Moreover, discounting or finite-time horizon based extension of the resolvent analysis has enabled resolvent analysis to study flows with unstable base states (Jovanović 2004; Yeh & Taira 2018). Because resolvent analysis can determine the most amplified forcing and response directions, it serves as a powerful analytical tool to find effective active and passive flow control techniques (Yeh & Taira 2018; Nakashima *et al.* 2017).

The resolvent analysis needs two key ingredients: (i) the base flow and (ii) the linearized Navier–Stokes operator. It is known that the accuracy of the base flow and the spatial discretization of the linear operators is also critical for extracting response characteristics correctly (Yeh & Taira 2018). The need for accurate discretization of the linearized Navier–Stokes operators calls for sufficient grid resolution and appropriate computational domain size. As such, the discrete resolvent operator becomes large with size $m \times m$, where m is essentially the number of variables times the size of the grid, which can easily be upward of $\mathcal{O}(10^6)$ for turbulent flows (Kajishima & Taira 2017). For resolvent analysis, the singular value decomposition (SVD) needs to be performed on the large resolvent operator with a taxing operation count of $\mathcal{O}(m^3)$. To enable resolvent analysis at high Reynolds numbers, we must find a relief to perform SVD of the resolvent operator.

Although the resolvent analysis is performed on a very large matrix, only the leading forcing and response modes are sought in general. Based on the amount of necessary matrix data used to perform the analysis, the desired output is only a very small fraction in terms of the input data size. For this reason, it would be natural to consider that all elements of the resolvent matrix are not necessary to determine the leading resolvent modes. One approach is to subsample the resolvent matrix and perform the analysis on the low-order representation of the resolvent operator. Randomized numerical linear algebra has recently emerged as an effective approach to reduce a large matrix to its low-order representation (Halko *et al.* 2011; Drineas & Mahoney 2016; Tropp *et al.* 2017), for applications such as big data compression and data transfer. The key idea is to pass a randomly generated low-rank test matrix through the large matrix to obtain the so-called sketch of the full matrix. This sketch is low-rank but holds key information about the full matrix and can be used to derive appropriate bases to represent the full matrix in a low-dimensional subspace (Woolfe *et al.* 2008; Halko *et al.* 2011; Tropp *et al.* 2017).

With the randomized technique, the leading singular values and modes can be determined in a computationally inexpensive manner, which is attractive for modal analysis in fluid mechanics. Thus far, randomized techniques have been incorporated into data-based modal analysis techniques, including the proper orthogonal decomposition (Rokhlin *et al.* 2009) and dynamic mode decomposition (Erichson *et al.* 2017). Here, we consider the use of randomized techniques for resolvent analysis. Although operator-based modal analysis techniques have traditionally been limited to moderate Reynolds number flows due to the size of the operators, the randomized technique presented below can greatly expand the applicability of the resolvent analysis to high-Reynolds number flows.

This paper is organized to introduce the randomized resolvent analysis in a concise manner. In section 2, we present the standard and randomized resolvent analyses. The randomized technique is then applied on a turbulent post-stall flow over a NACA 0012 airfoil in section 3. At last, we provide some concluding remarks in section 4.

2. Approach

2.1. Full resolvent analysis

Let us consider the flow state $\mathbf{q} \in \mathbb{R}^m$ as a sum of the time-invariant base state $\bar{\mathbf{q}}$ and the statistically stationary fluctuating component \mathbf{q}' . With this Reynolds decomposed

flow variable and appropriate discretization, we can express the discrete Navier–Stokes equations as

$$\frac{\partial \mathbf{q}'}{\partial t} = \mathbf{L}_{\bar{\mathbf{q}}} \mathbf{q}' + \mathbf{f}', \quad (2.1)$$

where $\mathbf{L}_{\bar{\mathbf{q}}} \in \mathbb{R}^{m \times m}$ is the linearized Navier–Stokes operator about the base state $\bar{\mathbf{q}}$ and \mathbf{f}' collects the nonlinear terms and the external forcing inputs. Traditionally, $\bar{\mathbf{q}}$ was chosen to be the stable laminar equilibrium state such that \mathbf{f}' from nonlinear terms would be negligible (Trefethen *et al.* 1993). In such case, \mathbf{f}' can be considered as the forcing input to the system (Jovanović & Bamieh 2005). More recently, turbulent mean flows has been used for $\bar{\mathbf{q}}$ with \mathbf{f}' representing the nonlinear terms as sustained forcing input within the natural feedback system (McKeon & Sharma 2010).

We can consider the Fourier transform $[\mathbf{q}'(\mathbf{x}, t), \mathbf{f}'(\mathbf{x}, t)] = \int_{-\infty}^{\infty} [\hat{\mathbf{q}}_{\omega}(\mathbf{x}), \hat{\mathbf{f}}_{\omega}(\mathbf{x})] e^{-i\omega t} d\omega$ and express the relationship between \mathbf{q}' and \mathbf{f}' in frequency space as

$$-i\omega \hat{\mathbf{q}}_{\omega} = \mathbf{L}_{\bar{\mathbf{q}}} \hat{\mathbf{q}}_{\omega} + \hat{\mathbf{f}}_{\omega}, \quad (2.2)$$

where ω is the frequency. Note that spatial Fourier transform can also be incorporated if directional homogeneity is present. For stable base flows, ω can be chosen to be real. To extend resolvent analysis to unstable base flows, we can consider the use of finite-time/discounted analysis (Jovanović 2004; Yeh & Taira 2018) by choosing a complex frequency $\omega = \omega_r + i\beta$, where both ω_r and β are real and β discounts the modal growth rate of $\mathbf{L}_{\bar{\mathbf{q}}}$. The input-output relationship between $\hat{\mathbf{f}}$ and $\hat{\mathbf{q}}$ can be found from (2.2) as

$$\hat{\mathbf{q}}_{\omega} = \mathbf{A} \hat{\mathbf{f}}_{\omega}, \quad (2.3)$$

where

$$\mathbf{A} = [-i\omega \mathbf{I} - \mathbf{L}_{\bar{\mathbf{q}}}]^{-1} \in \mathbb{C}^{m \times m} \quad (2.4)$$

is referred to as the *resolvent operator*. It serves as a transfer function that amplifies (or attenuates) the harmonic forcing input $\hat{\mathbf{f}}_{\omega}$ and maps it to the response $\hat{\mathbf{q}}_{\omega}$. The goal of resolvent analysis is to identify the dominant directions along which $\hat{\mathbf{f}}_{\omega}$ can be most amplified through \mathbf{A} to form the corresponding responses in $\hat{\mathbf{q}}_{\omega}$. This question is addressed by the SVD of

$$\mathbf{A} = \mathbf{U} \boldsymbol{\Sigma} \mathbf{V}^*, \quad (2.5)$$

where \mathbf{V}^* denotes the Hermitian of \mathbf{V} . Resolvent analysis interprets left and right singular vectors $\mathbf{U} = [\hat{\mathbf{u}}_1, \hat{\mathbf{u}}_2, \dots, \hat{\mathbf{u}}_m] \in \mathbb{C}^{m \times m}$ and $\mathbf{V} = [\hat{\mathbf{v}}_1, \hat{\mathbf{v}}_2, \dots, \hat{\mathbf{v}}_m] \in \mathbb{C}^{m \times m}$ respectively as response modes and forcing modes, with the magnitude-ranked singular values $\boldsymbol{\Sigma} = \text{diag}(\sigma_1, \sigma_2, \dots, \sigma_m) \in \mathbb{R}^{m \times m}$ being the amplification (gain) for the corresponding forcing-response pair. For unstable base flows, it is important that a finite-time window is chosen with β larger than the highest growth rate such that the resolvent analysis reveals the input-output relationship on a shorter time scale than that of the base flow instability.

Performing the SVD of $\mathbf{A} \in \mathbb{C}^{m \times m}$ requires an operation count of $\mathcal{O}(m^3)$, which is computationally taxing for large m . Such cases are encountered in high-Reynolds number and bi/tri-global analysis settings. However, we note that many applications of resolvent analysis call only for the dominant forcing and response modes $[\hat{\mathbf{v}}_1, \hat{\mathbf{u}}_1]$ associated with the highest gain σ_1 . This is appropriate when the first gain σ_1 is much larger than the rest of the gains $\sigma_{j>1}$ and shows a quick roll off. When the contributions from the higher-order modes are neglected, it is referred to as the rank-1 assumption for which the flow response is approximated as $\hat{\mathbf{q}} \approx \hat{\mathbf{u}}_1 \sigma_1 \langle \hat{\mathbf{v}}_1, \hat{\mathbf{f}} \rangle$, provided that $\sigma_1 \gg \sigma_2$ and $\hat{\mathbf{f}}$ has reasonable magnitude along $\hat{\mathbf{v}}_1$. In light of only seeking the dominant modal insights from

resolvent analysis, we present a remedy for performing large-scale resolvent analysis in a computationally tractable manner below.

2.2. Randomized resolvent analysis

With the assumption that a flow can be analyzed with the rank-1 approximation, we consider a low-rank representation of the resolvent operator \mathbf{A} . That is, instead of directly performing SVD for \mathbf{A} and obtaining the leading-mode representation, we seek a low-rank representation of \mathbf{A} and perform the SVD on the low-rank version of \mathbf{A} . We can consider finding an appropriate low-dimensional basis to project the large resolvent operator on a suitable subspace to derive the low-rank resolvent approximation.

The action of a full matrix on a vector should reveal some insights on which components are modified in the dominant directions. In the case of flow that can be described with the rank-1 approximation, there will be a low number of dominant directions. This very point can be taken advantage of through what is known as *sketching* in numerical linear algebra. Sketching refers to a procedure in which a tall and skinny test matrix $\Omega \in \mathbb{R}^{m \times k}$ (or $\mathbb{C}^{m \times k}$), where $k \ll m$, is passed through \mathbf{A}

$$\mathbf{Y} = \mathbf{A}\Omega. \quad (2.6)$$

Here, matrix $\mathbf{Y} \in \mathbb{C}^{m \times k}$ is called the *sketch* of matrix \mathbf{A} (Woolfe *et al.* 2008; Halko *et al.* 2011; Tropp *et al.* 2017). The test matrix Ω used in this work is a random matrix with standard normal Gaussian distribution (Martinsson *et al.* 2011). As the sketch Ω holds the dominant influence of \mathbf{A} , we can consider orthonormalizing \mathbf{Y} using a QR decomposition to form the orthonormal basis with $\mathbf{Q} \in \mathbb{C}^{m \times k}$ upon which we can project the full matrix \mathbf{A} to derive its low-rank approximation. In this way, it is possible to approximate \mathbf{A} for a rank $k \ll m$ as long as this approximation preserves the features of the leading modes. We also mention that the test matrix can be chosen to be the Radamacher distribution and even be sparse by allowing for the control of cost, stability and reliability in the operations (Tropp *et al.* 2017).

Given this \mathbf{Q} , a low-rank approximation of \mathbf{A} can be found as $\mathbf{A} \approx \mathbf{Q}\mathbf{Q}^*\mathbf{A}$ (Halko *et al.* 2011). We can view this as a low-rank decomposition of $\mathbf{A} \approx \mathbf{Q}\mathbf{B}$, where $\mathbf{B} = \mathbf{Q}^*\mathbf{A} \in \mathbb{C}^{k \times m}$. It is this reduced matrix \mathbf{B} upon which we can perform the SVD

$$\mathbf{B} = \tilde{\mathbf{U}}\Sigma\mathbf{V}^* \quad (2.7)$$

As a low-rank approximation, we now have

$$\mathbf{A} \approx \mathbf{Q}\tilde{\mathbf{U}}\Sigma\mathbf{V}^* \quad (2.8)$$

where we can consider $\mathbf{U} \approx \mathbf{Q}\tilde{\mathbf{U}}$. This process is the *randomized SVD* (Halko *et al.* 2011), where the sketch \mathbf{Y} was used to derive \mathbf{Q} . This approximation almost always satisfies $\|\mathbf{A} - \mathbf{Q}\mathbf{Q}^*\mathbf{A}\| \leq (1 + 9\sqrt{km})\sigma_{k+1}$. With this overall approach, the computational cost for SVD is reduced to $\mathcal{O}(mk^2)$ instead of $\mathcal{O}(m^3)$ for the full SVD. In our implementation, we use \mathbf{v}_1 from (2.8) and retrieve the leading singular value and left singular vector through

$$\mathbf{A}\hat{\mathbf{v}}_1 = \sigma_1\hat{\mathbf{u}}_1. \quad (2.9)$$

The singular value and vector can be separated by noticing that $\|\hat{\mathbf{u}}_1\| = 1$. The last equation provides more accurate leading singular value σ_1 and left singular vector $\hat{\mathbf{u}}_1$ compared to (2.8).

To utilize the randomized SVD for resolvent analysis, we must be aware that the resolvent operator \mathbf{A} contains an inverse operation in its definition (2.4), which need not be numerically performed. In the full resolvent analysis, one can only focus on modes

corresponding to the smallest singular values of \mathbf{A}^{-1} to find those for the largest singular values of \mathbf{A} . For the randomized resolvent analysis, the resolvent operator \mathbf{A} is needed for sketching \mathbf{Y} and to find the reduced \mathbf{B} . Unlike the original randomized SVD, matrix linear solvers can be employed to avoid calling for the inverse within the resolvent operator. The resulting algorithm constitutes the *randomized resolvent analysis* summarized below in Algorithm 1.

Algorithm 1 Randomized Resolvent Analysis

Require: inverse of the resolvent operator $\mathbf{A}^{-1} = [-i\omega\mathbf{I} - \mathbf{L}_{\bar{q}}] \in \mathbb{C}^{m \times m}$

```

1: function RAND_RESOLVENT( $k$ )
2:    $\Omega \leftarrow \text{randn}(m, k)$                                  $\triangleright$  random normal matrix generator
3:    $\mathbf{Y} \leftarrow [-i\omega\mathbf{I} - \mathbf{L}_{\bar{q}}] \setminus \Omega$        $\triangleright$  solve linear system for  $\mathbf{Y}$ ,  $\mathcal{O}(m^2k)$ 
4:    $(\mathbf{Q}, \sim) \leftarrow \text{qr}(\mathbf{Y}, 0)$                        $\triangleright$  economy-sized QR decomposition,  $\mathcal{O}(mk^2)$ 
5:    $\mathbf{B} \leftarrow \mathbf{Q}^* / [-i\omega\mathbf{I} - \mathbf{L}_{\bar{q}}]$                  $\triangleright$  solve linear system for  $\mathbf{B}$ ,  $\mathcal{O}(m^2k)$ 
6:    $(\sim, \sim, \mathbf{V}) \leftarrow \text{svd}(\mathbf{B}, \text{'econ'})$        $\triangleright$  reduced SVD decomposition,  $\mathcal{O}(mk^2)$ 
7:    $\mathbf{U}_{\Sigma} \leftarrow [-i\omega\mathbf{I} - \mathbf{L}_{\bar{q}}] \setminus \mathbf{V}$        $\triangleright$  recover  $\mathbf{U}_{\Sigma}$ ,  $\mathcal{O}(m^2k)$ 
8:   for  $i \leftarrow 1$  to  $k$  do
9:      $\Sigma(i, i) \leftarrow \text{norm}(\mathbf{U}_{\Sigma}(:, i), 2)$                  $\triangleright$  recover singular values  $\Sigma$ 
10:     $\mathbf{U}(:, i) \leftarrow \mathbf{U}_{\Sigma}(:, i) / \Sigma(i, i)$                    $\triangleright$  normalize  $\mathbf{U}$ 
11:   return  $(\mathbf{U}, \Sigma, \mathbf{V})$ 

```

With the randomized resolvent analysis, the SVD operation cost has been significantly reduced. The computational cost associated with each operation in the algorithm is also listed in Algorithm 1. We should point out that the cost of the three linear solvers are $\mathcal{O}(m^2k)$, which is a conservative upper bound. These costs can be further reduced if the properties of the resolvent operator can be taken advantage of to solve the linear system efficiently. We also note that the size of $\mathbf{B} \in \mathbb{C}^{k \times m}$ is considerably smaller than the original $\mathbf{A} \in \mathbb{C}^{m \times m}$ achieving a significant saving in freeing memory allocation during the SVD procedure. With the benefit of computational cost reduction and memory allocation relief, we now have a resolvent analysis algorithm that can accommodate problems with very large degrees of freedom.

3. Randomized resolvent analysis of post-stall turbulent flow

We demonstrate the use of randomized resolvent analysis on turbulent flow over a NACA 0012 airfoil. In this example, the randomized resolvent analysis will be applied a resolvent operator of size $m \times m$, where $m \simeq 7 \times 10^5$, to reveal the dominant gain and modal structures with a thin sketching matrix having as little as $k = 10$ columns. The convergence of the gain and resolvent modes will also be characterized with respect to the size of the sketching matrix. Influence of the ratio between the first and the second singular values of the resolvent operator will also be examined.

3.1. Problem setup

We consider the spanwise-periodic turbulent flow over a NACA 0012 airfoil at an angle of attack of 9° , a chord-based Reynolds number of $Re_{L_c} \equiv v_{\infty} L_c / \nu_{\infty} = 23,000$ and a free stream Mach number of $M_{\infty} \equiv v_{\infty} / a_{\infty} = 0.3$. Here, v_{∞} is the free-stream velocity, L_c is the chord length, a_{∞} is the free-stream sonic speed, and ν_{∞} is the kinematic viscosity. The time- and spanwise-averaged turbulent flow is considered as the base flow for the full and randomized resolvent analyses. For this 2D base flow, we adopt the bi-global setting that decomposes \mathbf{q}' into spanwise Fourier modes with the wavenumber k_z .

To obtain the base flow, large-eddy simulation (LES) is performed using a finite-volume compressible flow solver *CharLES* (Khalighi *et al.* 2011; Brès *et al.* 2017), which is

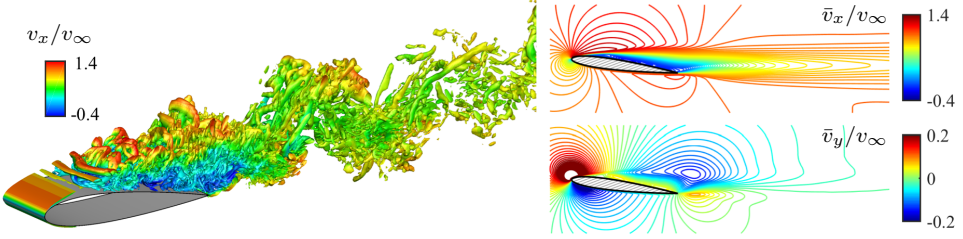


FIGURE 1. The instantaneous (left) and time/spanwise-averaged (right) flows over a NACA 0012 airfoil at $Re_{L_c} = 23,000$. The instantaneous flow visualization shows the isosurface of Q -Criterion ($QL_c^2/v_\infty^2 = 50$) colored by the instantaneous streamwise velocity.

second-order accurate in space and third-order accurate in time. The simulation has been validated with respect to the time-averaged pressure, lift and drag over the airfoil. The turbulent separated flow over the airfoil is visualized in figure 1. The visualization of the instantaneous flow shows the laminar separation from the leading edge. We have found that the shear layer physics dominates the pseudospectral behavior of the linearized Navier–Stokes operator, as shear is the main source of nonnormality in the operator. Further details regarding the computational setup, flow physics, and resolvent analysis based flow control of this flow are reported in Yeh & Taira (2018).

The full and randomized resolvent analyses are performed on a separate mesh from that used in the LES. This mesh has a 2D rectangular domain with the extent of $x/L_c \in [-15, 16]$ and $y/L_c \in [-12, 12]$, comprising approximately 0.15 million cells. Compared to the LES mesh, the mesh for resolvent analysis is coarser over the airfoil and in the wake, but is much finer in the upstream of the airfoil in order to resolve the forcing mode structures. The time- and spanwise-averaged flow \bar{q} obtained from LES is interpolated onto this mesh. At the far-field boundary and over the airfoil, Dirichlet condition is set for density and velocities and Neumann condition is prescribed for pressure in \mathbf{q}' . At the outlet boundary, Neumann condition is set for all flow variables. With these boundary conditions for \mathbf{q}' and the base flow \bar{q} , we construct the linearized Navier–Stokes operator $\mathbf{L}_{\bar{q}}(k_z)$ for a chosen k_z . The size of $\mathbf{L}_{\bar{q}}$ and the resolvent operator is approximately 0.75 million \times 0.75 million. While the SVD can be performed by simply calling the `svds` command in MATLAB package, it requires more than 120 gigabytes of memory for the resolvent operator of this size, which necessitates the use of high performance computing resource to conduct the full resolvent analysis.

3.2. Results

We perform the full and randomized resolvent analyses for spanwise wavenumbers of $k_z L_c = 0$ and 20π . Since the base flow is found to be unstable (Yeh & Taira 2018), the finite-time approach is adopted with $v_\infty/\beta L_c = 3$ to ensure that the resolvent analysis is performed on a shorter time scale than the dominant growth rate of the instability. For the randomized analysis, we consider $k = 10$ for the width of the test matrix Ω .

The leading forcing and response modes obtained from both full and randomized analyses are compared in figure 2 for representative frequencies St and spanwise wavelength $k_z L_c$. Although $k/m = 1.3 \times 10^{-5}$, we observe excellent agreement between the modes from the full resolvent analysis and the randomized algorithm for all cases. This remarkable level of agreement ensures that the randomized approach can provide great insights into the spatial structures to help understand the regions of sensitivity and guide flow control efforts. The modes are very similar for almost all frequencies and wavenumbers. In particular, background noise is perceived only in the forcing mode

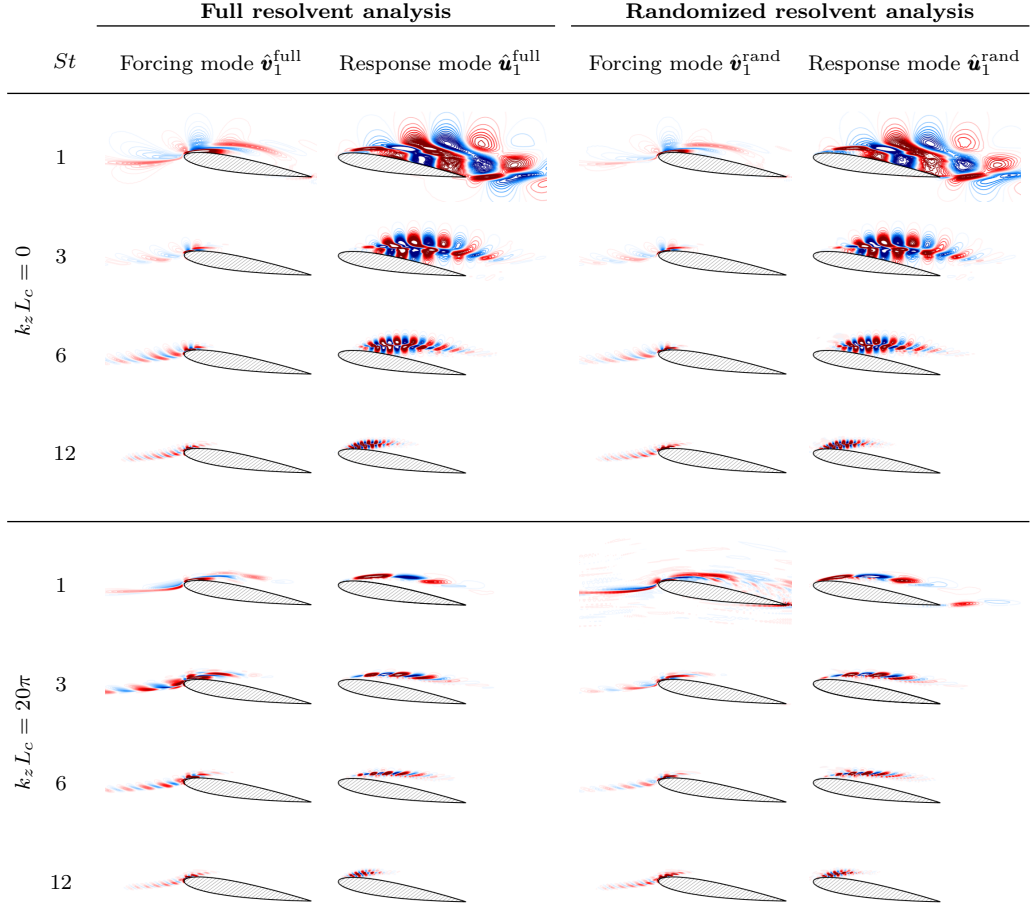


FIGURE 2. Leading forcing ($\hat{\mathbf{v}}_1$) and response ($\hat{\mathbf{u}}_1$) modes from the full and randomized resolvent analyses for $k_z L_c = 0$ and 20π at representative frequencies St . Modes are visualized with the streamwise velocity component with contour levels of $\hat{\mathbf{v}}_1/\|\hat{\mathbf{v}}_1\|_\infty$ and $\hat{\mathbf{u}}_1/\|\hat{\mathbf{u}}_1\|_\infty \in \pm[0.01, 0.6]$.

$\hat{\mathbf{v}}_1^{\text{rand}}$ for $k_z L_c = 20\pi$ and $St = 1$. However, the modal structures are still clearly visible even with the presence of noise. For this case, the randomized approach returns some structures emanating from the trailing edge in the response mode $\hat{\mathbf{u}}_1^{\text{rand}}$, which was not present from the full resolvent analysis. To shed light on this observation, we need to quantitatively assess this approximation.

The quantitative agreement between the full and randomized analyses with respect to the gain (leading singular value) and modes over a range of frequencies is shown in figure 3. The randomized analysis accurately captures the trend of gain distribution over $1 \lesssim St \lesssim 15$ in figure 3(a) for both wavenumbers. At the low and high-frequency ends, the gain shows deviations. The gain distribution is influenced by the eigenmodes associated with the shear-layer structure over the separation bubble (Yeh & Taira 2018). These eigenmodes are highly nonnormal and induce high-energy amplification through pseudoresonance (Trefethen *et al.* 1993). With the high-gain frequency range well captured, randomized resolvent analysis has demonstrated its capability of predicting the dominant pathway for energy amplification over the spectral space with a much lower computational cost.

The resemblance of the modal structure is quantified in figure 3(b) with the cosine

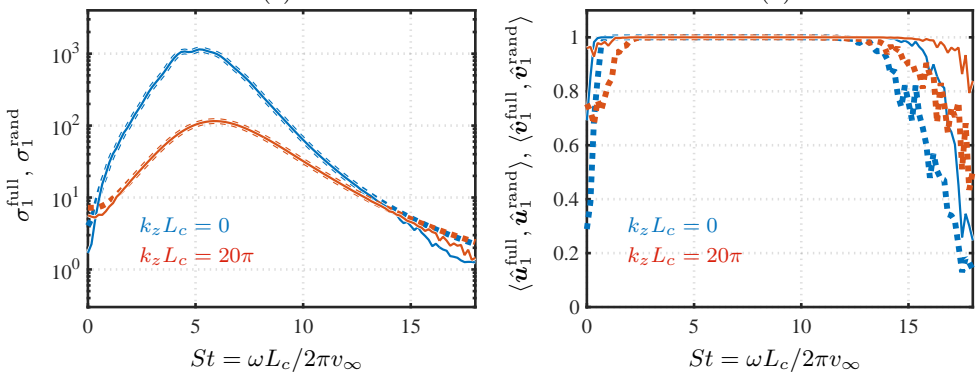


FIGURE 3. (a) Leading amplification for full (σ_1^{full} , dashed line) and randomized (σ_1^{rand} , solid line) resolvent analyses. (b) Cosine similarities for leading response $\langle \hat{u}_1^{\text{full}}, \hat{u}_1^{\text{rand}} \rangle$ (solid lines) and forcing $\langle \hat{v}_1^{\text{full}}, \hat{v}_1^{\text{rand}} \rangle$ (dashed lines) modes.

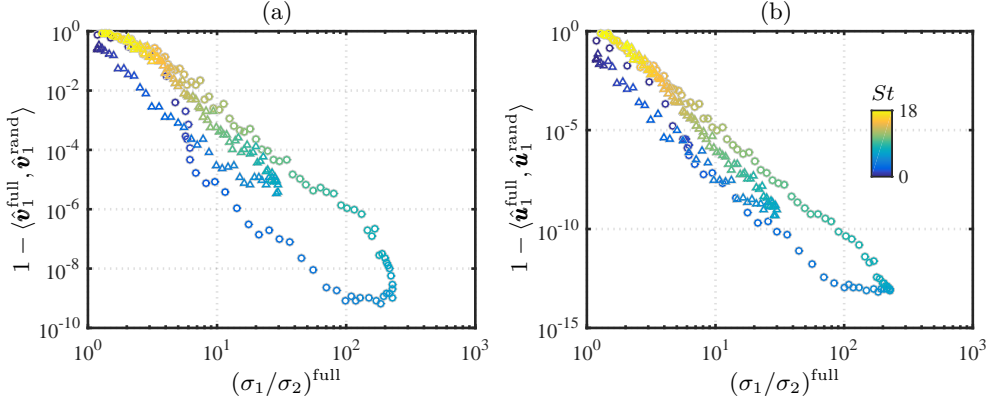


FIGURE 4. Error based on cosine similarity for the leading (a) forcing modes ($1 - \langle \hat{v}_1^{\text{full}}, \hat{v}_1^{\text{rand}} \rangle$) and (b) response modes ($1 - \langle \hat{u}_1^{\text{full}}, \hat{u}_1^{\text{rand}} \rangle$) over the leading gap from the full resolvent analysis. The symbols \circ and \triangle represent results from $k_z L_c = 0$ and 20π , respectively, colored by St .

similarities, i.e., the inner products, $\langle \hat{u}_1^{\text{full}}, \hat{u}_1^{\text{rand}} \rangle$ and $\langle \hat{v}_1^{\text{full}}, \hat{v}_1^{\text{rand}} \rangle$. As singular vectors are normalized, the cosine similarity of 1 suggests that perfect match is attained between the modes from full and randomized resolvent analyses. Since these modes are complex, the cosine similarity removes dependence on the phase difference. We observe that the randomized resolvent modes present a great agreement with the full resolvent modes. For almost the entire range of frequencies the cosine similarities are near unity. When this value is reduced, the modes may be affected by noise, as seen for \hat{v}_1^{rand} at $k_z L_c = 20\pi$ and $St = 1$ in figure 2.

As stated in section 2.2, the use of low-rank approximation in the randomized approach is built upon the assumption of the low-rank nature of the resolvent operator. The randomized resolvent analysis shows its strength when the singular values exhibit fast decay, as evident from figure 4. The accuracy of the modal structures captured by randomized analysis is examined with respect to the ratio of the leading and second singular values, $(\sigma_1/\sigma_2)^{\text{full}}$ from the full resolvent analysis. The error in the modal structures exhibits a decreasing trend as this ratio increases. When this ratio is close to unity, the randomized technique may not accurately separate the first and second modes. In fact, the aforementioned trailing edge structure that appeared in the randomized

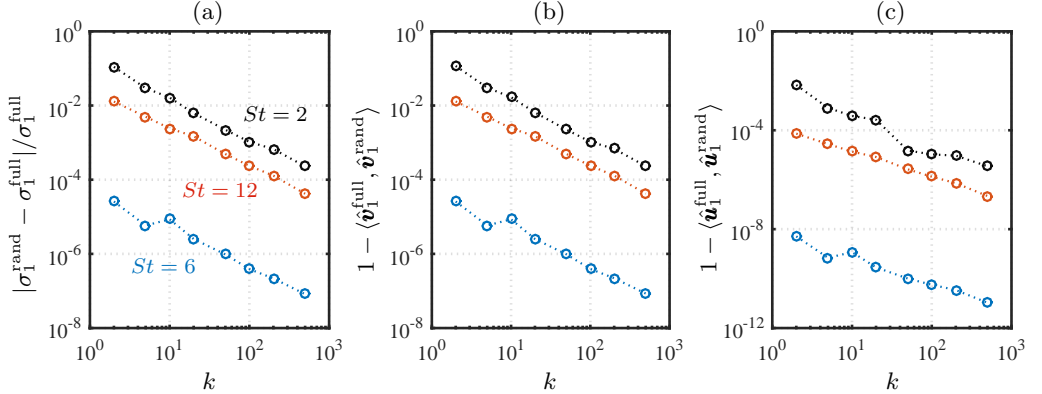


FIGURE 5. Influence of test matrix size k on the accuracy of (a) leading singular value, (b) forcing mode, and (c) response mode at $k_z L_c = 20\pi$. All exhibit $\mathcal{O}(k)$ convergence.

response mode for $k_z L_c = 20\pi$ and $St = 1$ is caused by the leakage of the structures from the second response mode (see figure 2). When the ratio $(\sigma_1/\sigma_2)^{\text{full}}$ is above 30, the error decreases to $\lesssim 10^{-5}$ for forcing modes and $\lesssim 10^{-8}$ for response modes.

Next, we study the influence of the width of the test matrix k on the error in leading singular values and modes, as presented in figure 5. When the value of k is varied from 2 to 500, the error from the use of randomized analysis decreases. For three representative frequencies, we observe the same rate of convergence $\approx \mathcal{O}(k)$ for both the gain and cosine similarity. For this flow, we observe that $k = 10$ is sufficient to achieve sufficient accuracy with $\lesssim 1\%$ error.

The overall randomized resolvent analysis has the operation count of $\mathcal{O}(m^2 k)$. For $k = 10$ (used in figures 2, 3 and 4), the memory usage of the randomized resolvent is approximately one quarter of the full resolvent analysis. Presently, the most intensive memory usage in the randomized technique appears from the naive use of the generic matrix solver in MATLAB. We can further reduce the computational and memory allocation needs by taking advantage of the properties of \mathbf{A} , e.g., utilization of an efficient linear solver using iterative methods. With the use of randomized numerical linear algebra, we are now empowered to perform the input-output analysis for ever more complex 2D and 3D turbulent base flows on a standard computer, or on a high-performance computing cluster to expand the envelop of resolvent analysis.

4. Conclusion

Resolvent analysis has proven to be a powerful technique to reveal the input-output characteristics of fluid flows. However, the computational cost and memory allocation of the technique can be taxing for high-Reynolds number flows, making it prohibitive to be applied to complex turbulent base flows. The major computational cost of the analysis is associated with the SVD of the resolvent operator. To remove this bottleneck, the randomized approach has been adopted to reduce the computational cost of SVD by considering the low-rank approximation of the resolvent operator. This was achieved by constructing the low-rank basis based on the insights gained from the sketch of the resolvent, which is obtained from a linear system solver. For flows with fast singular value decays, the randomized resolvent analysis reveals its power to accurately capture the response and forcing modes as well as the gain. To demonstrate the capability of the randomized resolvent analysis, we analyzed a turbulent separated flow over a NACA 0012 airfoil. We showed that the randomized technique finds the modes and the gain

with remarkable accuracy when the rank-1 approximation holds. Even for cases with close leading singular value spacing, the modal structures clearly identifies the response and forcing mode profiles. With the computational cost and memory allocation being relieved with the randomized approach, the applicability of the resolvent analysis can be significantly extended to higher-Reynolds number 2D and 3D base flows.

Acknowledgments

We gratefully acknowledge the support from the Air Force Office of Scientific Research (FA9550-18-1-0040), Army Research Office (W911NF-17-1-0118), and Office of Naval Research (N00014-16-1-2443). We thank L. Mathelin, S. L. Brunton, and N. B. Erichson for the enlightening discussions. Some of the computations presented here were supported by the Department of Defense High Performance Computing Modernization Program.

REFERENCES

BRÈS, G. A., HAM, F. E., NICHOLS, J. W. & LELE, S. K. 2017 Unstructured large-eddy simulations of supersonic jets. *AIAA Journal* **55** (4), 1164–1184.

DRINEAS, P. & MAHONEY, M. W. 2016 RandNLA: randomized numerical linear algebra. *Comm. ACM* **59** (6), 80–90.

ERICHSON, N. B., MATHELIN, L., KUTZ, J. N. & BRUNTON, S. L. 2017 Randomized dynamic mode decomposition. *available on arXiv in review*.

HALKO, N., MARTINSSON, P.-G. & TROPP, J. A. 2011 Finding structure with randomness: Probabilistic algorithms for constructing approximate matrix decompositions. *SIAM review* **53** (2), 217–288.

HOLMES, P., LUMLEY, J. L., BERKOOZ, G. & ROWLEY, C. W. 2012 *Turbulence, coherent structures, dynamical systems and symmetry*, 2nd edn. Cambridge Univ. Press.

JOVANOVIĆ, M. R. 2004 Modeling, analysis, and control of spatially distributed systems. PhD thesis, University of California at Santa Barbara, Dept. of Mechanical Engineering.

JOVANOVIĆ, M. R. & BAMIEH, B. 2005 Componentwise energy amplification in channel flows. *J. Fluid Mech.* **534**, 145–183.

KAJISHIMA, T. & TAIRA, K. 2017 *Computational fluid dynamics: incompressible turbulent flows*. Springer.

KHALIGHI, Y., NICHOLS, J. W., HAM, F., LELE, S. K. & MOIN, P. 2011 Unstructured large eddy simulation for prediction of noise issued from turbulent jets in various configurations. *AIAA Paper* 2011-2886.

MARTINSSON, P.-G., ROKHLIN, V. & TYGERT, M. 2011 A randomized algorithm for the decomposition of matrices. *Appl. Comput. Harmon. Anal.* **30** (1), 47–68.

MCKEON, B. J. & SHARMA, A. S. 2010 A critical-layer framework for turbulent pipe flow. *J. Fluid Mech.* **658**, 336–382.

NAKASHIMA, S., FUKAGATA, K. & LUHAR, M. 2017 Assessment of suboptimal control for turbulent skin friction reduction via resolvent analysis. *J. Fluid Mech.* **828**, 496–526.

ROKHLIN, V., SZLAM, A. & TYGERT, M. 2009 A randomized algorithm for principal component analysis. *SIAM J. Matrix Anal. Appl.* **31** (3), 1100–1124.

SCHMID, P. J. & HENNINGSON, D. S. 2001 *Stability and transition in shear flows*. Springer.

TAIRA, K., BRUNTON, S. L., DAWSON, S. T. M., ROWLEY, C. W., COLONIUS, T., MCKEON, B. J., SCHMIDT, O. T., GORDEYEV, S., THEOFILIS, V. & UKEILEY, L. S. 2017 Modal analysis of fluid flows: An overview. *AIAA J.* pp. 4013–4041.

THEOFILIS, V. 2011 Global linear instability. *Annu. Rev. Fluid Mech.* **43**, 319–352.

TREFETHEN, L. N., TREFETHEN, A. E., REDDY, S. C. & DRISCOLL, T. A. 1993 Hydrodynamic stability without eigenvalues. *Science* **261** (5121), 578–584.

TROPP, J. A., YURTSEVER, A., UDELL, M. & CEVHER, V. 2017 Practical sketching algorithms for low-rank matrix approximation. *SIAM J. Matrix Anal. Appl.* **38** (4), 1454–1485.

WOOLFE, F., LIBERTY, E., ROKHLIN, V. & TYGERT, M. 2008 A fast randomized algorithm for the approximation of matrices. *Appl. Comput. Harmon. Anal.* **25**, 335366.

YEH, C.-A. & TAIRA, K. 2018 Resolvent-analysis-based design of airfoil separation control. *J. Fluid Mech.* *in review*.